1-21-2016

The 40-Residue Insertion in Vibrio Cholerae FadR Facilitates Binding of an Additional Fatty acyl-CoA Ligand

Wei Shi
Dartmouth College

Gabriela Kovacikova
Dartmouth College

Wei Lin
Dartmouth College

Ronald. K. Taylor
Dartmouth College

Karen Skorupski
Dartmouth College

See next page for additional authors

Published in final edited form as:
Nat Commun. ; 6: 6032. doi:10.1038/ncomms7032.

The 40-residue insertion in *Vibrio cholerae* FadR facilitates binding of an additional fatty acyl-CoA ligand

Wei Shi[2], **Gabriela Kovacikova**[3], **Wei Lin**[3], **Ronald K. Taylor**[3], **Karen Skorupski**[3], and **F. Jon Kull**[1,2]

[1]Department of Chemistry, Dartmouth College, Geisel School of Medicine at Dartmouth, Hanover, New Hampshire, USA

[2]Department of Biochemistry, Geisel School of Medicine at Dartmouth, Hanover, New Hampshire, USA

[3]Department of Microbiology and Immunology, Geisel School of Medicine at Dartmouth, Hanover, New Hampshire, USA

Abstract

FadR is a master regulator of fatty acid metabolism and influences virulence in certain members of *Vibrionaceae*. Among FadR homologs of the GntR family, the *Vibrionaceae* protein is unusual in that it contains a C-terminal 40-residue insertion. Here we report the structure of *Vibrio cholerae* FadR (*Vc*FadR) alone, bound to DNA, and in the presence of a ligand, oleoyl-CoA. Whereas *Escherichia coli* FadR (*Ec*FadR) contains only one acyl-CoA binding site in each monomer, crystallographic and calorimetric data indicate that *Vc*FadR has two. One of the binding sites resembles that of *E. coli* FadR, whereas the other, comprised of residues from the insertion, has not previously been observed. Upon ligand binding, *Vc*FadR undergoes a dramatic conformational change that would more fully disrupt DNA binding than *Ec*FadR. These findings suggest that the ability to bind and respond to an additional ligand allows FadR from *Vibrionaceae* to function as a more efficient regulator.

Introduction

In all organisms, fatty acids (FAs) are essential components of membranes and important sources of metabolic energy. FadR is a member of the GntR family of transcription factors that coordinately controls the pathways of FA degradation and unsaturated fatty acid (UFA) biosynthesis in enteric bacteria[1]. In the absence of exogenous long chain fatty acids

Correspondence should be addressed to F.J.K. (f.jon.kull@dartmouth.edu).

Author Contributions

W.S. purified, crystalized the *Vc*FadR, *Vc*FadR-DNA complex and *Vc*FadR-ligand complex and also collected data on the crystals and determined the structures. W.S. performed ITC experiments and analyzed the data. G.K and W.L. constructed the *V. cholerae* plasmids and strains and carried out the β-galactosidase assays. K.S., R.K.T. and F.J.K. were involved in study conception and study design. The manuscript was prepared by W.S., K.S., and F.J.K.

Accession codes: Atomic coordinates and structure factor files have been deposited in the Protein Data Bank (ID codes: apo-*Vc*FadR, 4P96; *Vc*FadR-DNA complex, 4P9U; *Vc*FadR-ligand complex, 4PDK).

Competing financial interests: The authors declare no competing financial interests.

(LCFAs), FadR functions as a repressor of FA degradation by binding to a site in the promoters of the *fad* genes and interfering with RNA polymerase[2] (Fig. 1a). These genes include *fadL*, *fadD*, *fadBA*, *fadE*, and *fadH* that encode proteins required for the transport, activation and β-oxidation of LCFAs[3]. In *V. cholerae*, FadR also represses the expression of the *plsB* gene involved in membrane phospholipid biosynthesis[4]. In the absence of exogenous LCFAs, FadR simultaneously activates the expression of the *fabA* and *fabB* genes that encode proteins required for the biosynthesis of UFAs[5,6]. When exogenous LCFAs are present (Fig. 1b), they are transported across the outer membrane by FadL and activated by the inner membrane-associated acyl-coenzyme A (CoA) ligase FadD[7] to produce long chain fatty acyl-CoAs (LCFA-CoAs). These LCFA-CoAs bind directly to FadR and induce a conformational change that releases FadR from its binding sites[8]. This derepresses *fad* gene expression to utilize the LCFAs and decreases the expression of *fabA* and *fabB* since UFA biosynthesis is no longer necessary.

In addition to controlling the activity of FadR, UFAs, which are components of bile in the intestinal lumen, are important signals present in the host environment that influence the expression of virulence genes in *V. cholerae*[9]. Members of *Vibrionaceae* are ubiquitous in marine and fresh water environments, with species found in open water, estuaries and marine sediments as either free-living or in association with phyto- and zooplankton[10,11]. *Vibrio cholerae* is the causative agent of the acute intestinal infection cholera. Upon entry into the host intestine, *V. cholerae* induces a transcriptional cascade resulting in the expression of the AraC-type master virulence regulator, ToxT. ToxT directly activates the expression of the two primary virulence factors of *V. cholerae*, the toxin-coregulated pilus (TCP)[12] and cholera toxin (CT)[13]. UFAs have been found to directly bind into the pocket of ToxT and influence its activity by impairing the ability of the protein to dimerize and bind to DNA[14]. The location of the UFA, buried in the ligand pocket at the interface between the N- and C- terminal domains is thought to promote a “closed” conformation of ToxT that is not capable of binding to DNA. Once the bacteria have penetrated the mucus of the intestine, and the concentrations of UFAs are reduced, the closed conformation is presumably destabilized, and the protein becomes competent for DNA binding and activation of gene expression[14].

The majority of FadR proteins that have been identified are members of the GntR family, as typified by *E. coli* FadR (*Ec*FadR), which has been crystallized in its apo, ligand-bound, and DNA-bound forms[15–17]. *Ec*FadR has an N-terminal DNA binding domain containing a winged helix-turn-helix (wHTH) motif, and a C-terminal domain consisting of a seven-helical bundle containing a large cavity that is involved in acyl-CoA binding[15]. Upon ligand binding, effector induced conformational changes occur in the protein that lead to displacement of the entire DNA binding domain with respect to the effector binding domain, leading to disruption of the protein-DNA complex[16].

FadR from *Vibrionaceae* is unusual among FadRs of the GntR family in that it contains a 40 amino acid insertion in its C-terminal domain[18]. Although FadR from *V. cholerae* appears to repress gene expression as well as other FadR homologs that have been examined, it has a higher binding affinity for acyl-CoAs than the other homologs and it induces the expression of genes involved in FA utilization (i.e. it is derepressed) more efficiently in the presence of

ligand[18]. It has been suggested that these properties may be related to the 40 amino acid insertion confined to the family. To gain insights into the role of this 40 amino acid insertion for *V. cholerae* FadR (*Vc*FadR), we have crystallized the *Vc*FadR protein in three forms: apo, bound to its cognate DNA, and in the presence of a ligand, oleoyl-CoA. Our results indicate the insertion region in *Vc*FadR potentially stabilizes the wing of the wHTH DNA binding domain in the absence of DNA and, strikingly, facilitates the binding of a second oleoyl-CoA ligand in each monomer. The large conformational changes that occur in the protein upon binding of this second ligand are predicted to more fully disrupt DNA binding than what has been observed in the *E. coli* protein, possibly explaining why *Vc*FadR is a more efficient regulatory protein.

Results

*Vc*FadR is unusual but still regulates FA metabolism

FadR is present in a variety of bacterial species where it plays a role in the transcriptional regulation of genes involved in FA metabolism[19]. The regulation of genes involved in FA degradation and UFA biosynthesis by FadR in *V. cholerae* has been inferred from bioinformatics analyses[19,20]. To confirm that *Vc*FadR functions as a regulator of these processes in *V. cholerae*, fusions of a promoterless *lacZ* gene from *E. coli* were made to the upstream regions of the *V. cholerae fadBA*, *fadE*, and *fadH* genes involved in FA degradation and to the *fabA* and *fabB* genes involved in UFA biosynthesis. The fusions were introduced into the *V. cholerae* chromosome at the *lacZ* locus, and examined in the presence and absence of FadR and LCFAs. As shown in Fig. 1c, the loss of FadR increased the expression of the *fadBA*, *fadE* and *fadH* promoters 2, 2.8 and 2.5 fold, respectively, whereas it decreased the expression of the *fabA* and *fabB* promoters 6.7 and 4.5 fold, respectively, in the absence of LCFAs. In the presence of LCFAs (Fig. 1d), no significant difference in the expression of the fusions was observed between the wild-type and Δ*fadR* mutant strains. These results show that FadR functions as a regulator of FA metabolism in *V. cholerae*.

*Vc*FadR shares 52% sequence identity with *Ec*FadR (Fig. 2a). However, the protein from *V. cholerae*, as well as from other members of *Vibrionaceae*, shows a major difference from all other GntR family FadRs that have been sequenced in that it contains 40 additional residues in the C-terminal domain (Figs 2a, b and Supplementary Fig.1). A Blast search[21] with *V. cholerae* FadR also reveals several related proteins with a 44-residue insertion (Supplementary Fig. 1). Thus, it appears that *Vibrionaceae* FadRs acquired an insertion at some point in their evolution; retention of this insertion suggests it provides a biological advantage for the organism.

Structure of apo-*Vc*FadR and comparison with *Ec*FadR

To shed light on the role of the insertion for *Vibrionaceae*, the structure of *V. cholerae* apo-FadR was determined (Fig. 3a and Table 1). The asymmetric unit contains a dimer formed in a manner similar to that of *Ec*FadR (PDB 1E2X and 1HW1)[15,17]. Each monomer consists of an α/β N-terminal domain (residues 2–72, α1-β1-α2-α3-β2-W1-β3-W2, ‘W’ denotes a ‘wing’), a helical C-terminal domain (residues 94–279, α5–α6–αI1-αI2-α7-α8–α9–α10, ‘I’ denotes that the helix is derived from the insertion), and a short helical linker (residues 81–

89, α4) (Fig. 3a). The structure of the N-terminal domain conforms to the so-called wHTH motif[22], consistent with its role in binding DNA, and contains the most flexible loop in the structure as suggested by its B-factors (Supplementary Fig. 2a).

Superposition of the *Vc*FadR dimer onto the *Ec*FadR dimer (PDB 1E2X)[15] (Fig. 3b) reveals that overall the two proteins are very similar [root mean square deviation (RMSD) over 424 alpha carbon atoms is 1.64 Å] except for the insertion (residues 138–177), which lies between helix α6 and helix α7. The insertion region elongates helices α6 and α7, as previously predicted[18], and forms two additional short α-helices, αI1 and αI2, along with several connecting loops.

Structure of *Vc*FadR with DNA and comparison with *Ec*FadR

*Vc*FadR was crystallized in complex with a 31-bp oligonucleotide derived from the *V. cholerae fadBA* promoter (Figs 4a, b, and Table 1). As in the *Ec*FadR-DNA complex (PDB 1H9T and 1HW2)[16,17], the DNA binding site is recognized by residues from helices α1, α2, and α3, which interact with the major groove, as well as the two wings (W1 and W2) that bind to the adjacent minor grooves (Figs 4a, c), stabilizing these loops significantly (Supplementary Fig. 2b). As in the *Ec*FadR-DNA complex, the DNA in the *V. cholerae* FadR-DNA complex has a B-form conformation with a curvature of ~20° toward the protein, resulting in a contraction of the central major groove and an expansion of the opposite minor groove. As the amino acid sequences of the DNA binding domains of the *V. cholerae* and *E. coli* proteins are nearly identical (Fig. 2a), the protein-DNA contacts are also very similar. For example, there are five residues in both proteins that specifically recognize DNA base pairs (R35 in α2; R45 and T46 in α3; and H65 and G66 in the tip of the wing) (Figs 4b, c and Supplementary Fig. 3). There are also similarities in a number of nonspecific interactions with the DNA sugar-phosphate backbone, including A9, E34, T44, T47, R49 and T69 (Figs 4b, c and Supplementary Fig. 3). All contacts are symmetrical, except for T44, H65 and G66 (which have both symmetrical and non-symmetrical contacts) and K67 (which only has a non-symmetrical contact) (Fig. 4b).

Superposition of the structures of the dimeric *Vc*FadR-DNA complex and the apo-*Vc*FadR dimer (Fig. 5a) shows that the DNA binding domain and the insertion region are altered upon DNA binding. Within the DNA binding domain, the distance between the two DNA recognition helices (α3) narrows from 17 Å in the apo-*Vc*FadR structure to 15 Å in the *Vc*FadR-DNA complex such that it is better able to interact with the DNA (Fig. 5a). In addition, the tip of the wing in each wHTH DNA binding domain is shifted by 5 Å, forming interactions with DNA (Fig. 5a).

Although the insertion region (αI1, αI2 and several connecting loops) does not directly contact DNA (Fig. 5a), it undergoes a conformational change upon DNA binding. In the absence of DNA, the wing of the wHTH of chain A interacts with αI2 from the insertion region of chain B (Fig. 5b) via hydrogen bonds between the side chains of Q64 and K67 and the carbonyl oxygen of Q1592 (residues from chain B are distinguished by a prime) and two salt bridges (K70-E1552 and E76-K1562), suggesting the insertion stabilizes the wing. These interactions are also symmetric, although the distances are slightly longer between the insertion of chain A and the wing of chain B. In the presence of DNA (Fig. 5c), the wing of

the wHTH moves away from the insertion to interact with DNA and helices αI1, αI2 and the C-terminal end of α6 undergo a helix to loop transition. This conformational change in the insertion region when *Vc*FadR is bound to DNA may be due to the loss of interactions with the wing.

Structure of *Vc*FadR with ligand and comparison with *Ec*FadR

In order to visualize the effects of ligand binding on *Vc*FadR, the structure was determined in the presence of the high binding affinity ligand, oleoyl-CoA[18] (18:1) (Figs 6a, b, and Table 1). Interestingly, in contrast to *Ec*FadR, which binds one molecule of ligand [myristoyl-CoA (14:0) (PDB 1H9G)[16]] per monomer (Fig. 6c), *Vc*FadR binds two ligand molecules, with one (colored pink in Fig. 6a) located in the site corresponding to the *Ec*FadR ligand binding site (designated site #1) and the other (colored yellow in Fig. 6a) in a binding site derived in part from the 40-residue insertion region (designated site #2) that is structurally distinct from site #1 (electron density is shown in Supplementary Fig. 4). Thus, the insertion in FadR from *Vibrionaceae* facilitates the binding of a second molecule of ligand into each monomer; this has not been observed in any FadR structure that has been solved to date.

For the ligand bound to site #1 in monomer A, salt bridges are formed between ligand phosphates and residues R253, K1182 and R2452 (Figs 6d, Supplementary Fig. 5a). In monomer B, the phosphorylated adenosine head group of the site #1 ligand has a different and more disordered conformation than that in monomer A (Supplementary Fig. 6), and electron density can be observed for multiple positions of the head group. The arrangements of salt bridges in *Vc*FadR differ significantly from the *Ec*FadR-myristoyl-CoA structure (1H9G)[16] where only one salt bridge forms between the ligand phosphate and *Ec*FadR R213 (corresponding to *Vc*FadR R253). In *Vc*FadR, additional hydrogen bonds are formed between carbonyl oxygens in the pantothenic acid moiety and the polar side chains T106 and S259 (Fig. 6d and Supplementary Fig. 5a), homologous to hydrogen bonds involving *Ec*FadR T106 and S219). Finally, as in the *Ec*FadR-myristoyl-CoA structure (1H9G)[16], the C18 acyl chain adopts a bent conformation and terminates in a hydrophobic pocket formed by residues L101, I108 and L208 from helices α5 and α8 (Figs 6d and Supplementary Fig. 5a). The FadR ligand pocket thus can clearly accommodate ligands of different lengths, as the longer acyl chain in *Vc*FadR structure extends ~4 Å farther into the pocket compared with the C14 acyl chain of myristoyl-CoA in *Ec*FadR (1H9G)[16]. It is unclear from the structure if the unsaturated bond between C9 and C10 of oleoyl-CoA plays an important role in binding, however comparison of the *Vc*FadR and *Ec*FadR pockets in this region does show one change that might be significant; M168 in *Ec*FadR is replaced by L208 in *Vc*FadR, which is positioned relatively further away from the ligand, perhaps to accommodate the kink in the fatty acyl chain introduced by the double bond (Supplementary Fig. 7)

For ligand binding site #2, residues involved in specific interactions with the ligand are shown in Fig. 6e and Supplementary Fig. 5b. Both K156 from αI2 and R191 from α7 form salt bridges with ligand phosphate groups, and Y153 from αI2 forms a π-stacking interaction with the adenine ring. N130, S134, and Y184 form hydrogen bonds with the

adenine ring (Fig. 6e). The C18 acyl chain is buried in a pocket surrounded by hydrophobic residues and the tails of the acyl chains from each monomer pack closely together (Fig. 6a, right-center). The dominantly hydrophobic pocket is mainly formed by residues from helix α8 and the loop region connecting the DNA-binding and the ligand binding domains (e.g. I822, I832, I200, L203, G207) (Fig. 6e and Supplementary Fig. 5b). In addition, upon ligand binding, residues in the DNA binding domain (e.g. W212, P272) move closer to the C-terminal domain and interact with the ligand (see following section). Interestingly, the bent helix α8 (residues 199–221, notably G207) forms part of both binding sites #1 and #2. The above-mentioned residues that are interacting with ligand in binding site #2 are highly conserved among the other FadR proteins with the insertion (Fig. 2b and Supplementary Fig. 1), suggesting that they will also bind the second ligand.

To determine the thermodynamic parameters for binding of the oleoyl-CoA ligand to *Vc*FadR, isothermal titration calorimetry (ITC) was used to measure the dissociation constant (K_d), enthalpy (ΔH), and the stoichiometry of binding (n). Typical ITC profiles of the binding of oleoyl-CoA to *Vc*FadR are shown in Supplementary Fig. 8. Consistent with the crystal structure, the stoichiometry of binding indicates that every monomer of *Vc*FadR protein binds two molecules of oleoyl-CoA. The biphasic nature of the isotherm indicates the presence of nonequivalent binding sites with different affinities for oleoyl-CoA (6 nM and 88 nM). Although it is not possible to determine which binding site has the higher affinity from the ITC data, computed scoring functions obtained from X-SCORE[23] and DSX[24] predict the higher affinity binding pocket to be site #1.

Comparison of effector mediated conformational changes

Having defined the structures of *V. cholerae* apo-FadR, FadR-DNA and FadR-oleoyl-CoA ligand complexes, a comparison can now be made between the effects of ligand binding on *Vc*FadR and *Ec*FadR. In *Vc*FadR, the linker helix α4, which is observed in the *Vc*FadR-DNA and apo-*Vc*FadR structures (Figs 7a, b and Supplementary Fig. 9), unwinds upon ligand binding to site #2 to avoid potential clashes with the ligand (Supplementary Fig. 2c). This transition also appears to destabilize the extensive hydrophobic contacts of α4 with the adjacent DNA binding and the ligand binding domains (Supplementary Fig. 9c), enabling the DNA binding domain to become uncoupled from the ligand binding domain.

Comparison of the *Vc*FadR-oleoyl-CoA and *Vc*FadR-DNA complexes shows that ligand binding induces the DNA binding domain to move as a rigid body towards the C-terminal domain (Fig. 7c). This allows residues W212 and P272 from the DNA binding domain to interact with the ligand (Figs 6e, 7c); in turn, this could stabilize the DNA binding domain in this conformation. This movement leads to a large change in the distance between the two recognition helices (α3), from 15 Å in the *Vc*FadR-DNA complex (17 Å in the apo-*Vc*FadR structure) to 65 Å in *Vc*FadR-oleoyl-CoA complex (Fig. 7c and Supplementary Fig. 10a). Based on these conformational changes, we propose that binding of the second ligand to *Vc*FadR induces a dramatic separation of the two recognition helices, strongly inhibiting the ability of *Vc*FadR to interact with DNA.

In contrast to *Vc*FadR, ligand binding to *Ec*FadR does not alter the conformation of linker helix α4 as significantly. Instead of the unwinding of α4 described above, ligand binding to

*Ec*FadR pushes α4 towards the N-terminal DNA binding domain, where it forms additional contacts with helix α1. The resulting tilt in α1 moves the DNA binding domain ~13° away from the DNA[16]. This results in smaller separation of the two recognition helices of *Ec*FadR than observed in *Vc*FadR; from 15Å in the *Ec*FadR-DNA complex (PDB 1H9T; 15Å in the apo-*Ec*FadR structure, PDB 1E2X)[15,16] to 23Å in the *Ec*FadR-myristoyl-CoA structure (PDB 1H9G)[16] (Fig. 7d and Supplementary Fig. 10b).

Discussion

FadR is the master regulator of FA metabolism in bacteria and coordinately controls the pathways of FA degradation and UFA biosynthesis. In *V. cholerae*, FadR also regulates these processes, but the protein is different from other GntR family homologs in that it has a 40-residue insertion in its C-terminal domain. In all of the structures of FadR that have been solved to date, each monomer binds only one molecule of the acyl-CoA ligand. Although the overall structure of *Vc*FadR and the manner in which it binds to DNA described here is similar to *Ec*FadR, the insertion in the *V. cholerae* protein elongates the acyl-CoA binding domain and accommodates a second ligand of oleoyl-CoA. One of these sites (site #1) is structurally similar to the ligand binding site in *Ec*FadR whereas the other (site #2) is comprised of residues from the insertion as well as from the N- and C- terminal domains of the protein. Although the two sites share some structural features, such as the involvement of residues within α8, *Vc*FadR appears to have evolved a new way to bind an additional molecule of the same ligand.

We are aware of only two other transcription factors that have been shown to bind more than one molecule of the same ligand in distinct sites within a monomer. The *E. coli* catabolite gene activator protein (CAP) was crystallized in the presence of DNA with two molecules of cAMP bound to each monomer (PDB 2CGP); however it is not clear if binding of the second ligand is biologically relevant[25]. BenM, a LysR family transcription factor, was also crystallized with one molecule of benzoate bound at a primary site and another molecule of benzoate (PDB 2F78) bound at a secondary binding site within the same monomer; however, a different ligand, muconate, is also capable of binding at the primary site[26]. In the presence of both effectors, a unique conformation capable of high level transcriptional activation is achieved[26].

The two ligand binding sites in *Vc*FadR appear to have significantly different affinities for oleoyl-CoA. Site #1, the site structurally similar to *Ec*FadR, is predicted to be the higher affinity site and appears to bind ligand with a higher affinity (6 nM) than the *E. coli* protein, determined for oleoyl-CoA to be 70 nM. In contrast, site #2, derived from the insertion, is predicted to be the lower affinity site and binds ligand with a reduced affinity (88 nM) compared to the *E. coli* protein. Both site #1 and #2 of *Vc*FadR bind ligand with a higher affinity compared to S. enterica (143 nM), P. multocida (2231 nM) and H. influenzae protein (2636 nM)[18]. Analysis of *Vc*FadR binding site #1 shows a greater number of salt bridges are formed with ligand phosphates than for *Ec*FadR, and these additional interactions could be responsible for the increased affinity for ligand at this site. It is also possible that the presence of the insertion in *Vc*FadR alters the dynamics of the entire protein so as to increase the affinity for ligand at site #1[27]. For example, in addition to providing a

second binding site for the ligand, the insertion also appears to stabilize the wing of the wHTH binding domain in the absence of DNA. This interaction could change the protein such that its affinity for ligand increases.

It has previously been shown that addition of oleate to *V. cholerae* FadR allows for nearly complete derepression of genes involved in FA utilization, suggesting that in the presence of ligand, *Vc*FadR decreases its affinity for DNA to a greater extent than other regulators[18]. These findings are consistent with our observation that the *V. cholerae* protein undergoes dramatic conformational changes upon ligand binding that would more fully disrupt DNA binding than the ligand induced movements in *Ec*FadR and suggest that the binding of ligand to site #2 is physiologically relevant. In *Vc*FadR, ligand binding to site #2 induces a helix to loop transition in α4 that enables the DNA binding domain to swing towards the C-terminal domain, forming stabilizing interactions with the site #2 ligand. We propose this conformational change allows for a more complete release of the protein from the DNA, leading to fuller expression of the FA utilization genes. In addition, the presence of two binding sites with different affinities likely gives *Vc*FadR a broader response range to different concentrations of ligand than *Ec*FadR. For example, the model predicts that, at very low concentrations, *Vc*FadR binds only one ligand per monomer (likely at site #1) causing *Vc*FadR to have a reduced affinity for DNA, similar to that of *Ec*FadR. At higher concentrations of ligand, *Vc*FadR binds two ligands per monomer (at both sites #1 and #2) further reducing the affinity of the protein for DNA in comparison to *Ec*FadR. Unlike other enteric bacteria such as *E. coli* that colonize the digestive tract, *Vibrionaceae* are frequently found in aquatic environments where they acquire FAs from the sediment[28,29]. The need for *Vibrionaceae* to have a more efficient mechanism for utilizing FAs in this environment may have selected for an additional ligand binding site in FadR that allows the protein to function as a more dynamic regulatory switch.

Methods

Expression and purification of FadR

V. cholerae FadR was purified using the IMPACT-CN fusion protein system (New England Biolabs). The full-length *fadR* gene was PCR amplified from *V. cholerae* C6706 str2 using primers FadR5 and FadR6 (Supplementary Table 1). The resulting fragment was inserted into pTXB1 (New England Biolabs) to produce the FadR-intein/CBD (chitin binding domain) fusion construct pWEL225. FadR was expressed in BL21 (DE3) by autoinduction[30] in ZYM-5052 media. Cells were harvested by centrifugation, resuspended in column buffer (20 mM HEPES pH 7.8, 1 mM EDTA, and 500 mM NaCl), lysed by sonication, clarified by centrifugation, and filtered through a 0.45 μm filter. Chitin beads (New England Biolabs) were equilibrated with cold column buffer, mixed with the clarified supernatant, and incubated at 4°C with gentle rocking. The chitin bead slurry was then loaded onto a gravity flow column, washed with 50 column volumes of high salt wash buffer (20 mM HEPES pH 7.8, 1 mM EDTA, and 1 M NaCl), and equilibrated with five column volumes of cleavage buffer (20 mM HEPES pH 7.8, 1 mM EDTA, and 50 mM NaCl). The intein with the CBD was cleaved from FadR using cleavage buffer with 100 mM β-mercaptoethanol and left at 16 °C for 16 h. Eluant from the chitin column in cleavage buffer was then loaded onto a new

chitin column and followed by a HiTrap Sepharose prepacked (Q) fast flow (FF) strong anionic exchange column (GE) using a NaCl gradient. This separates the FadR-intein/CBD fusion protein and the intein tag that coeluted with the native FadR. The fractions containing FadR were identified by SDS-polyacrylamide gel electrophoresis and pooled. The pooled fractions were concentrated with an Amicon Ultra Centrifugal filter unit (Millipore) and applied to a Superdex 75 Prep Grade column (GE) equilibrated in crystallization buffer (20 mM HEPES pH 7.8, 1 mM EDTA, and 100 mM NaCl). FadR eluted as a single peak at a position consistent with a dimer and was essentially pure as judged by SDS-polyacrylamide gel electrophoresis.

To prepare the *Vc*FadR-DNA complex for crystallization, the oligonucleotides WS1 and WS2 (Supplementary Table 1) were dissolved in low salt buffer (100 mM NaCl and 10 mM NaOH) and purified by MonoBeads prepacked Mono Q strong anionic exchange column (GE) with a NaCl gradient in 10 mM NaOH. The fractions containing pure oligonucleotides were pooled and concentrated as described above and the buffer was exchanged into crystallization buffer by a desalting column (GE). The purified oligonucleotides were annealed, concentrated and applied to a Superdex 75 Prep Grade column (GE) equilibrated in crystallization buffer to eliminate unannealed oligonucleotides. The purified dsDNA was mixed with purified *Vc*FadR at a protein/DNA ratio of 1:1.5. The *Vc*FadR-DNA complexes were concentrated as described above and applied to a Superdex 200 Prep Grade column (GE) equilibrated in crystallization buffer. The fractions containing the *Vc*FadR-DNA complexes were collected and concentrated as described above.

Crystallization

Crystals of apo-*Vc*FadR were obtained using the sitting drop procedure by mixing equal volumes of the protein solution at 6 mg/ml with a reservoir solution containing 0.2 M sodium chloride, 0.1 M MES pH 6.5, 10% (w/v) PEG 4000. Crystals typically grew within 1 week. *Vc*FadR crystals were cryoprotected in a 30% v/v solution of glycerol/mother liquor and flash frozen in liquid nitrogen for X-ray data collection. Crystals of the *Vc*FadR-DNA complex were also obtained by the sitting drop method by mixing equal volumes of 8 mg/ml complex solution with a reservoir containing 0.2 M lithium sulfate, 0.1 M Tris pH 8.5, 1.26 M ammonium sulfate. Crystals grew in 2 weeks. *Vc*FadR-DNA complex crystals were cryoprotected in a 30% v/v solution of glycerol/mother liquor and flash frozen in liquid nitrogen for X-ray data collection. Crystals of the *Vc*FadR-oleoyl-CoA complex, also obtained by the sitting drop method, were produced by mixing equal volumes of *Vc*FadR-ligand complex (*Vc*FadR=4 mg/ml; ligand (oleoyl coenzyme A lithium salt (Sigma))/ *Vc*FadR monomer molar ratio=3.6:1) solution with a reservoir containing 17% PEG 3350, 0.23 M magnesium formate. Crystals grew in about 1 week. *Vc*FadR-oleoyl-CoA complex crystals were cryoprotected in a 30% v/v solution of glycerol/mother liquor and flash frozen in liquid nitrogen for X-ray data collection.

Data collection and structure solution

Crystals of apo-*Vc*FadR diffracted to 2.2 Å at NSLS beamline X6A at Brookhaven National Laboratory. Crystals belonged to the tetragonal space group $P4^1$ with unit cell dimensions a=87.48 Å, b=87.48 Å, c=81.43 Å, α=90.0°,β=90.0°, γ=90.0°. The asymmetric unit

contained one dimer of *Vc*FadR, giving a crystal volume per protein mass (V_M) of 2.4 Å^3/Da and a solvent content of 49.7%. Data were processed in XDS[31] and structure determination was carried out using AutoMR in Phenix[32]. Two copies of the *E. coli* FadR monomer divided into the N-terminal (residues 6 to 137) and C-terminal domain (residues 138 to 226) were used as search models for molecular replacement. The insertion region was built back manually in Coot[33]. Multiple rounds of refinement and rebuilding were carried out in Phenix.refine[34] and Coot[33], respectively, using data to 2.2 Å. The resulting final structure has a R-work 17.44% of and R-free of 20.46% with good stereochemistry (Table 1) and continuous density for the backbone from residue 2 to 279 out of 279 possible residues (Fig. 3a). Ramachandran statistics show that 97% and 2.82% of the residues are in the preferred and allowed regions, respectively. In MOLPROBITY[35] validation results, this structure was assigned a MOLPROBITY score of 1.44, which is the 99th percentile among structures of comparable resolution.

Diffraction data for the *Vc*FadR-DNA complex were collected to 3.2 Å at NSLS beamline X6A at Brookhaven National Laboratory. Crystals belonged to the triclinic space group P1 with unit cell dimensions a=84.6 Å, b=94.7 Å, c=101.7 Å, α=89.8°, β=114.6°, γ=116.5°. The asymmetric unit contained two molecules of *Vc*FadR-DNA complex, giving a crystal volume per protein mass (V_M) of 3.9 Å^3/Da and a solvent content of 71.0%. Data were processed in XDS[31] and structure determination was carried out using AutoMR in Phenix[32]. Four copies of the *V. cholerae* FadR monomer without the insertion region and two copies of DNA from *E. coli* FadR-DNA complex were used as search models for molecular replacement. The resulting maps showed density for the insertion region and density for additional DNA duplex. The insertion region was built back manually in Coot[33]; the DNA duplex was mutated to the *V. cholerae* FadR DNA sequence and additional bases were built back manually in Coot[33]. Multiple rounds of refinement and rebuilding were carried out in Phenix.refine[34] and Coot[33], respectively, using data to 3.2 Å. The resulting final structure has a R-work of 21.76% and R-free of 25.23%, with good stereochemistry (Table 1) and continuous density that included all atoms in DNA and residues from residue 6 to 277 out of 279 possible residues (Fig. 4a). Ramachandran statistics show that 91% and 7.6% of the residues are in the preferred and allowed regions, respectively. In MOLPROBITY[35] validation results, this structure was assigned a MOLPROBITY score of 2.55, which is the 96th percentile among structures of comparable resolution.

Diffraction data for *Vc*FadR with ligand were collected to 2.8 Å at NSLS beamline X6A at Brookhaven National Laboratory. Crystals belonged to the orthorhombic space group $P2_12_12_1$ with unit cell dimensions a=116.92 Å, b=88.69 Å, c=62.86 Å, α=90°, β=90°, γ=90°. The asymmetric unit contained one dimer of *Vc*FadR-oleoyl-CoA complex, giving a crystal volume per protein mass (V_M) of 2.4 Å^3/Da and a solvent content of 48.4%. Data were processed in XDS[31] and structure determination was carried out using AutoMR in Phenix[32]. Initial molecular replacement with *V. cholerae* apo-FadR as a search model, was unsuccessful, suggesting that significant structural rearrangement might have occurred upon binding of oleoyl-CoA. Subsequent molecular replacement with only the C-terminal acyl-CoA binding domain gave a single solution. Refinement in Phenix[34] resulted in maps in which the ligands and the N-terminal DNA binding domain could be positioned manually in

Coot[33]. Multiple rounds of refinement and rebuilding were carried out in Phenix.refine[34] and Coot[33], respectively, using data to 2.8 Å. The resulting final structure has a R-work of 25.57% and R-free of 30.35%, with good stereochemistry (Table 1) and continuous density that included all atoms in the ligand and residues from residue 8 to 266 out of 279 possible residues (Fig. 5b). Ramachandran statistics show that 87% and 6.8% of the residues are in the preferred and allowed regions, respectively. In MOLPROBITY[35] validation results, this structure was assigned a MOLPROBITY score of 3.15, which is the 53rd percentile among structures of comparable resolution.

Construction of *V. cholerae* strains and mutations

The *fabA-lacZ* fusion was constructed by amplifying a DNA fragment from C6706 str2 using primers FabA1 and FabA3 (Supplementary Table 1). The fragment, together with a promoterless *lacZ* fragment from pVC200[36], were inserted into pKAS180[37] generating pWEL234. Plasmid pWEL234 was used for allelic exchange[37] into the *lacZ* locus of *V. cholerae* strain KSK262[38] generating WL1005. Plasmid pWEL236 was constructed by amplifying a DNA fragment from C6706 str2 using primers Chr1 and Chr2 and a DNA fragment from pVC200[36] using primers LacNot and LacBgl. The resulting fragments were inserted into pKAS154[39]. The *fadE, fadBA, fadH and fabB-lacZ* fusions were constructed by amplifying DNA fragments from C6706 str2 using primers FadE1 and FadE3, FadB1 and FadB4, and FadH1 and FadH3, and FabB3 and FabB4. The resulting fragments were inserted into pWEL236, generating plasmids pWEL239, pWEL240, pWEL242, and pGKK469, respectively. The fusions in the resulting plasmids were introduced into the *lacZ* locus of KSK262 by allelic exchange generating strains WL1027, WL1031, WL1040, and GK1609. The Δ*fadR* mutation was constructed by amplifying two DNA fragments from C6706 str2 using primers FadR1 with FadR2 and FadR3 with FadR4. The fragments were inserted into pKAS154[39], generating plasmid pGKK367, and the deletion was introduced into the chromosome of *V. cholerae* by allelic exchange.

β-Galactosidase assays

β-Galactosidase assays[40] were carried out by growing cultures in Tryptone medium with aeration for 5 h at 37°C.

Supplementary Material

Refer to Web version on PubMed Central for supplementary material.

Acknowledgements

This work was supported by National Institutes of Health Grant AI072661 (to F.J.K) and Grant AI039654 (to R.K.T). Research carried out at the X6A beam line was funded by the NIH (NIGMS) under agreement GM-0080. We thank the staff of National Synchrotron Light Source (NSLS) beamline X6A, particularly V. Stojanoff and E. Lazo, for beam time and help with data collection; D. Wilcox and M. Carpenter for training, guidance, and usage of the VP-ITC; S. Almagro-Moreno for helpful discussions and critical reading of the manuscript and our colleagues in the Kull laboratory for intellectual discussions. The authors also thank John Cronan for strains and immunoreagents for the detection of FadR, as well as insightful discussions.

References

1. Zhang YM, Rock CO. Transcriptional regulation in bacterial membrane lipid synthesis. J. Lipid Res. 2009; 50(Suppl):S115–S119. [PubMed: 18941141]
2. Cronan JE Jr, Subrahmanyam S. FadR, transcriptional co-ordination of metabolic expediency. Mol. Microbiol. 1998; 29:937–943. [PubMed: 9767562]
3. Clark, DP.; Cronan, JE, Jr. Escherichia coli and Salmonella : cellular and molecular biology. Neidhardt, Frederick C., editor. ASM Press; 1996. p. 343p. 357
4. Feng Y, Cronan JE. The *Vibrio cholerae* fatty acid regulatory protein, FadR, represses transcription of *plsB*, the gene encoding the first enzyme of membrane phospholipid biosynthesis. Mol. Microbiol. 2011; 81:1020–1033. [PubMed: 21771112]
5. Henry MF, Cronan JE Jr. *Escherichia coli* transcription factor that both activates fatty acid synthesis and represses fatty acid degradation. J. Mol. Biol. 1991; 222:843–849. [PubMed: 1722255]
6. Campbell JW, Cronan JE Jr. *Escherichia coli* FadR positively regulates transcription of the *fabB* fatty acid biosynthetic gene. J. Bacteriol. 2001; 183:5982–5990. [PubMed: 11566998]
7. DiRusso CC, Black PN. Bacterial long chain fatty acid transport: gateway to a fatty acid-responsive signaling system. J. Biol. Chem. 2004; 279:49563–49566. [PubMed: 15347640]
8. DiRusso CC, Heimert TL, Metzger AK. Characterization of FadR, a global transcriptional regulator of fatty acid metabolism in Escherichia coli. Interaction with the *fadB* promoter is prevented by long chain fatty acyl coenzyme A. J. Biol. Chem. 1992; 267:8685–8691. [PubMed: 1569108]
9. Chatterjee A, Dutta PK, Chowdhury R. Effect of fatty acids and cholesterol present in bile on expression of virulence factors and motility of *Vibrio cholerae*. Infect. Immun. 2007; 75:1946–1953. [PubMed: 17261615]
10. Reen FJ, Almagro-Moreno S, Ussery D, Boyd EF. The genomic code: inferring *Vibrionaceae* niche specialization. Nat. Rev. Microbiol. 2006; 4:697–704. [PubMed: 16894340]
11. Takemura AF, Chien DM, Polz MF. Associations and dynamics of *Vibrionaceae* in the environment, from the genus to the population level. Front. Microbiol. 2014; 5:38. [PubMed: 24575082]
12. Taylor RK, Miller VL, Furlong DB, Mekalanos JJ. Use of *phoA* gene fusions to identify a pilus colonization factor coordinately regulated with cholera toxin. Proc. Natl. Acad. Sci. U.S.A. 1987; 84:2833–2837. [PubMed: 2883655]
13. Waldor MK, Mekalanos JJ. Lysogenic conversion by a filamentous phage encoding cholera toxin. Science. 1996; 272:1910–1914. [PubMed: 8658163]
14. Lowden MJ, et al. Structure of *Vibrio cholerae* ToxT reveals a mechanism for fatty acid regulation of virulence genes. Proc. Natl. Acad. Sci. U.S.A. 2010; 107:2860–2865. [PubMed: 20133655]
15. van Aalten DM, DiRusso CC, Knudsen J, Wierenga RK. Crystal structure of FadR, a fatty acid-responsive transcription factor with a novel acyl coenzyme A-binding fold. EMBO J. 2000; 19:5167–5177. [PubMed: 11013219]
16. van Aalten DM, DiRusso CC, Knudsen J. The structural basis of acyl coenzyme A-dependent regulation of the transcription factor FadR. EMBO J. 2001; 20:2041–2050. [PubMed: 11296236]
17. Xu Y, Heath RJ, Li Z, Rock CO, White SW. The FadR.DNA complex. Transcriptional control of fatty acid metabolism in *Escherichia coli*. J. Biol. Chem. 2001; 276:17373–17379. [PubMed: 11279025]
18. Iram SH, Cronan JE. Unexpected functional diversity among FadR fatty acid transcriptional regulatory proteins. J. Biol. Chem. 2005; 280:32148–32156. [PubMed: 16027119]
19. Kazakov AE, et al. Comparative genomics of regulation of fatty acid and branched-chain amino acid utilization in proteobacteria. J. Bacteriol. 2009; 191:52–64. [PubMed: 18820024]
20. Sadovskaya NS, Laikova ON, Mironov AA, Gelfand MS. Study of regulation of long-chain fatty acid metabolism using computer analysis of complete bacterial genomes. Mol. Biol. 2001; 35:1010–1014.
21. Altschul SF, Gish W, Miller W, Myers EW, Lipman DJ. Basic local alignment search tool. J. Mol. Biol. 1990; 215:403–410. [PubMed: 2231712]

22. Gajiwala KS, Burley SK. Winged helix proteins. Curr. Opin. Struct. Biol. 2000; 10:110–116. [PubMed: 10679470]
23. Wang R, Lai L, Wang S. Further development and validation of empirical scoring functions for structure-based binding affinity prediction. J. Comput. Aided Mol. Des. 2002; 16:11–26. [PubMed: 12197663]
24. Neudert G, Klebe G. DSX: a knowledge-based scoring function for the assessment of protein-ligand complexes. J. Chem. Inf. Model. 2011; 51:2731–2745. [PubMed: 21863864]
25. Passner JM, Steitz TA. The structure of a CAP-DNA complex having two cAMP molecules bound to each monomer. Proc. Natl. Acad. Sci. U.S.A. 1997; 94:2843–2847. [PubMed: 9096308]
26. Ezezika OC, Haddad S, Clark TJ, Neidle EL, Momany C. Distinct effector-binding sites enable synergistic transcriptional activation by BenM, a LysR-type regulator. J. Mol. Biol. 2007; 367:616–629. [PubMed: 17291527]
27. Motlagh HN, Wrabl JO, Li J, Hilser VJ. The ensemble nature of allostery. Nature. 2014; 508:331–339. [PubMed: 24740064]
28. Giles DK, Hankins JV, Guan Z, Trent MS. Remodelling of the *Vibrio cholerae* membrane by incorporation of exogenous fatty acids from host and aquatic environments. Mol. Microbiol. 2011; 79:716–728. [PubMed: 21255114]
29. Urakawa H, Yoshida T, Nishimura M, Ohwada K. Characterization of depth-related population variation in microbial communities of a coastal marine sediment using 16S rDNA-based approaches and quinone profiling. Environ. Microbiol. 2000; 2:542–554. [PubMed: 11233162]
30. Studier FW. Protein production by auto-induction in high density shaking cultures. Protein Expr. Purif. 2005; 41:207–234. [PubMed: 15915565]
31. Kabsch W. Xds. Acta Crystallogr. D Biol. Crystallogr. 2010; 66:125–132. [PubMed: 20124692]
32. McCoy AJ, et al. Phaser crystallographic software. J. Appl. Crystallogr. 2007; 40:658–674. [PubMed: 19461840]
33. Emsley P, Cowtan K. Coot: model-building tools for molecular graphics. Acta Crystallogr. D Biol. Crystallogr. 2004; 60:2126–2132. [PubMed: 15572765]
34. Afonine PV, et al. Towards automated crystallographic structure refinement with phenix.refine. Acta Crystallogr. D Biol. Crystallogr. 2012; 68:352–367. [PubMed: 22505256]
35. Chen VB, et al. MolProbity: all-atom structure validation for macromolecular crystallography. Acta Crystallogr. D Biol. Crystallogr. 2010; 66:12–21. [PubMed: 20057044]
36. Parsot C, Mekalanos JJ. Expression of ToxR, the transcriptional activator of the virulence factors in *Vibrio cholerae*, is modulated by the heat shock response. Proc. Natl. Acad. Sci. U.S.A. 1990; 87:9898–9902. [PubMed: 2124707]
37. Skorupski K, Taylor RK. Positive selection vectors for allelic exchange. Gene. 1996; 169:47–52. [PubMed: 8635748]
38. Kovacikova G, Skorupski K. A *Vibrio cholerae* LysR homolog, AphB, cooperates with AphA at the *tcpPH* promoter to activate expression of the ToxR virulence cascade. J. Bacteriol. 1999; 181:4250–4256. [PubMed: 10400582]
39. Kovacikova G, Skorupski K. Regulation of virulence gene expression in *Vibrio cholerae* by quorum sensing: HapR functions at the *aphA* promoter. Mol. Microbiol. 2002; 46:1135–1147. [PubMed: 12421317]
40. Miller, JH. Experiments in molecular genetics. Cold Spring Harbor Laboratory; 1972.
41. Larkin MA, et al. Clustal W and Clustal X version 2.0. Bioinformatics. 2007; 23:2947–2948. [PubMed: 17846036]
42. Gouet P, Robert X, Courcelle E. ESPript/ENDscript: Extracting and rendering sequence and 3D information from atomic structures of proteins. Nucleic Acids Res. 2003; 31:3320–3323. [PubMed: 12824317]
43. Gui L, Sunnarborg A, LaPorte DC. Regulated expression of a repressor protein: FadR activates *iclR*. J. Bacteriol. 1996; 178:4704–4709. [PubMed: 8755903]

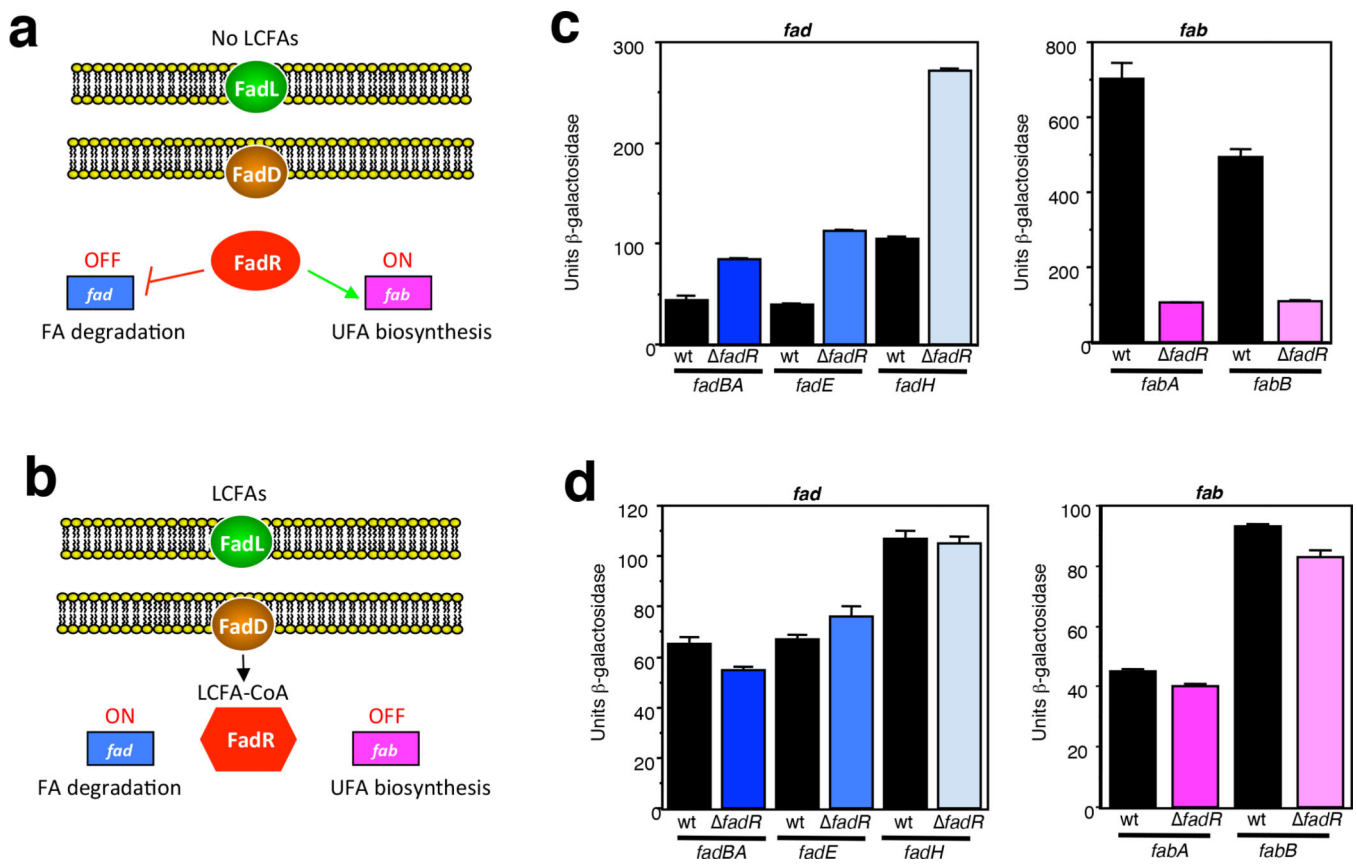

Figure 1. Roles of FadR in *V. cholerae*

(a, b) Schematic showing FadR-mediated regulation in *V. cholerae*. In the absence of LCFAs, (a), FadR represses FA degradation by binding to a site in the promoters of the *fad* genes and activates UFA biosynthesis by binding to a site in the promoters of the *fabA* and *fabB* genes. In the presence of LCFAs, (b), they are transported into the cell by FadL and activated to LCFA-CoAs by FadD. The resulting activated LCFA-CoAs bind to FadR causing a conformational change that releases it from DNA and results in derepression and failure to activate its regulated promoters. (c, d) Influence of a Δ*fadR* mutation on the expression of *fadBA, fadE, fadH, fabA and fabB* promoter-*lacZ* fusions in *V. cholerae*. Strains were grown in Tryptone medium with aeration for 5 h at 37°C in the absence (c) and presence (d) of 2.5 mM oleate. From left to right: WL1031 (*fadBA-lacZ*), WL1035 (Δ*fadR*), WL1027 (*fadE-lacZ*), WL1029 (Δ*fadR*), WL1040 (*fadH-lacZ*), WL1042 (Δ*fadR*), WL1005 (*fabA-lacZ*), WL1007 (Δ*fadR*), GK1609 (*fabB-lacZ*), GK1610 (Δ*fadR*). Error bars indicate the standard deviation of at least two replicates. Results are representative of at least three independent experiments.

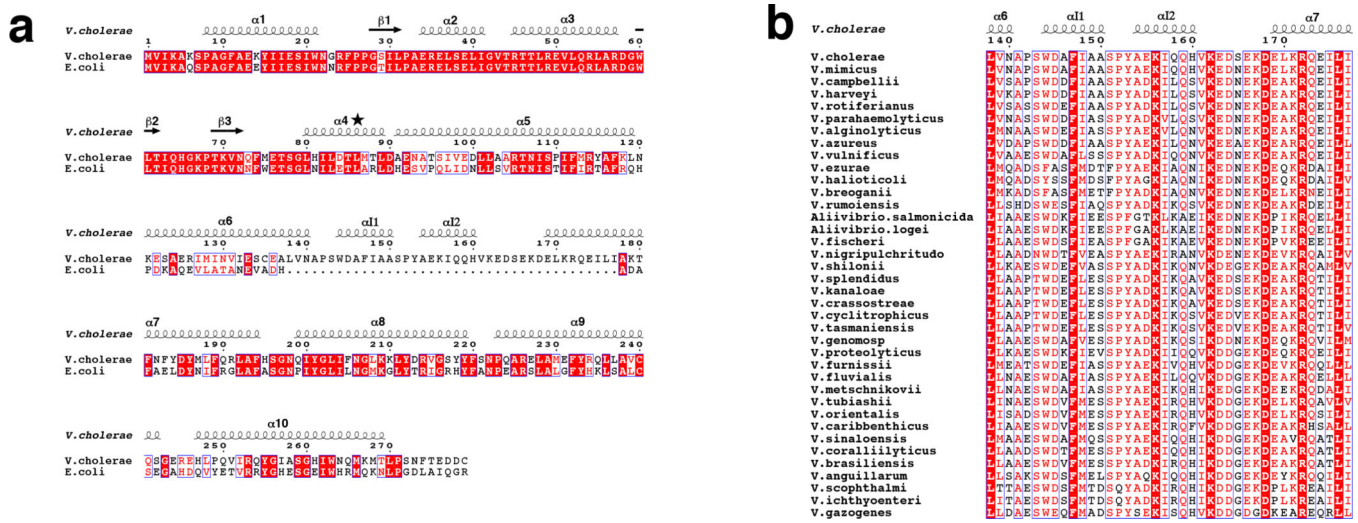

Figure 2. Sequence alignment of FadR

(a) Alignment of FadR between *V. cholerae* and *E. coli*. Identical residues are indicated by red background. Incomplete identities among aligned sequences are in red text. Secondary structure is shown above the sequence and the numbering is based on *Ec*FadR (PDB 1E2X)[15]. Helix α4, marked with the star, undergoes a helix to loop transition upon ligand binding. (b) Alignment of 40-residue insertions from *Vibrionaceae*. Colors are the same as in (a). The alignments were prepared with Clustal W[41] and ESPript 3.0[42] (http://espript.ibcp.fr/).

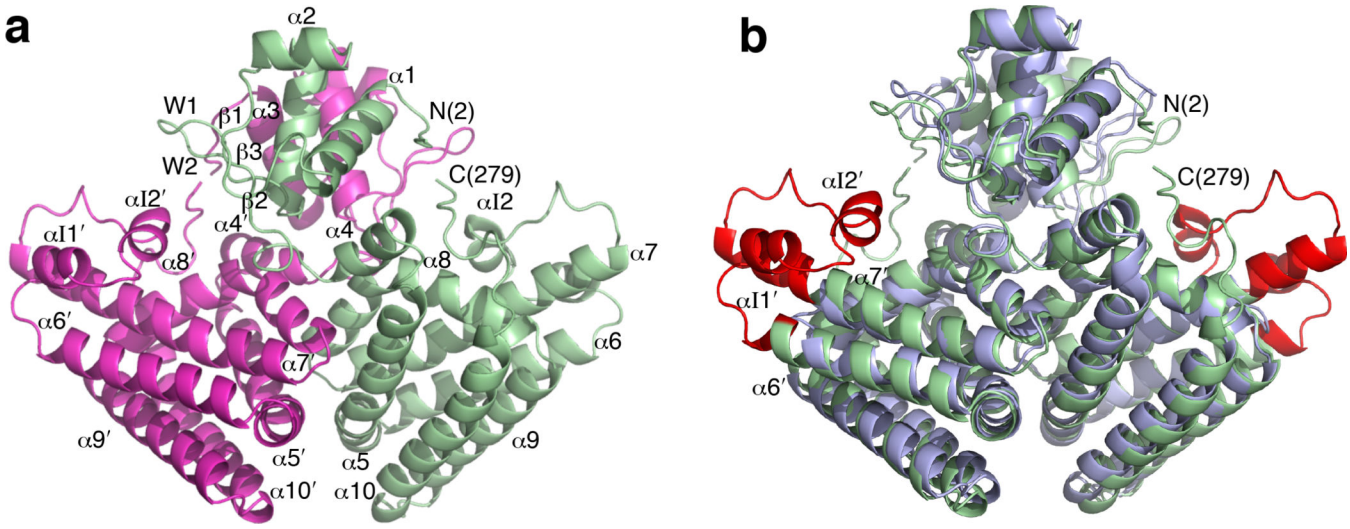

Figure 3. Structure of *Vc*FadR

(a) The *Vc*FadR dimer. One monomer is magenta and the other is green. The N and C termini are labeled and the amino acid positions are shown in parentheses. αI1 and αI2 denote the helices from the insertion and W1 and W2 denote wings. Helices from chain B are distinguished by a prime. (b) Superposition of the structures of the *Vc*FadR and *Ec*FadR dimers (PDB 1E2X). The 40-residue insertion in *Vc*FadR is red and the rest of the protein is green. *Ec*FadR is shown in blue.

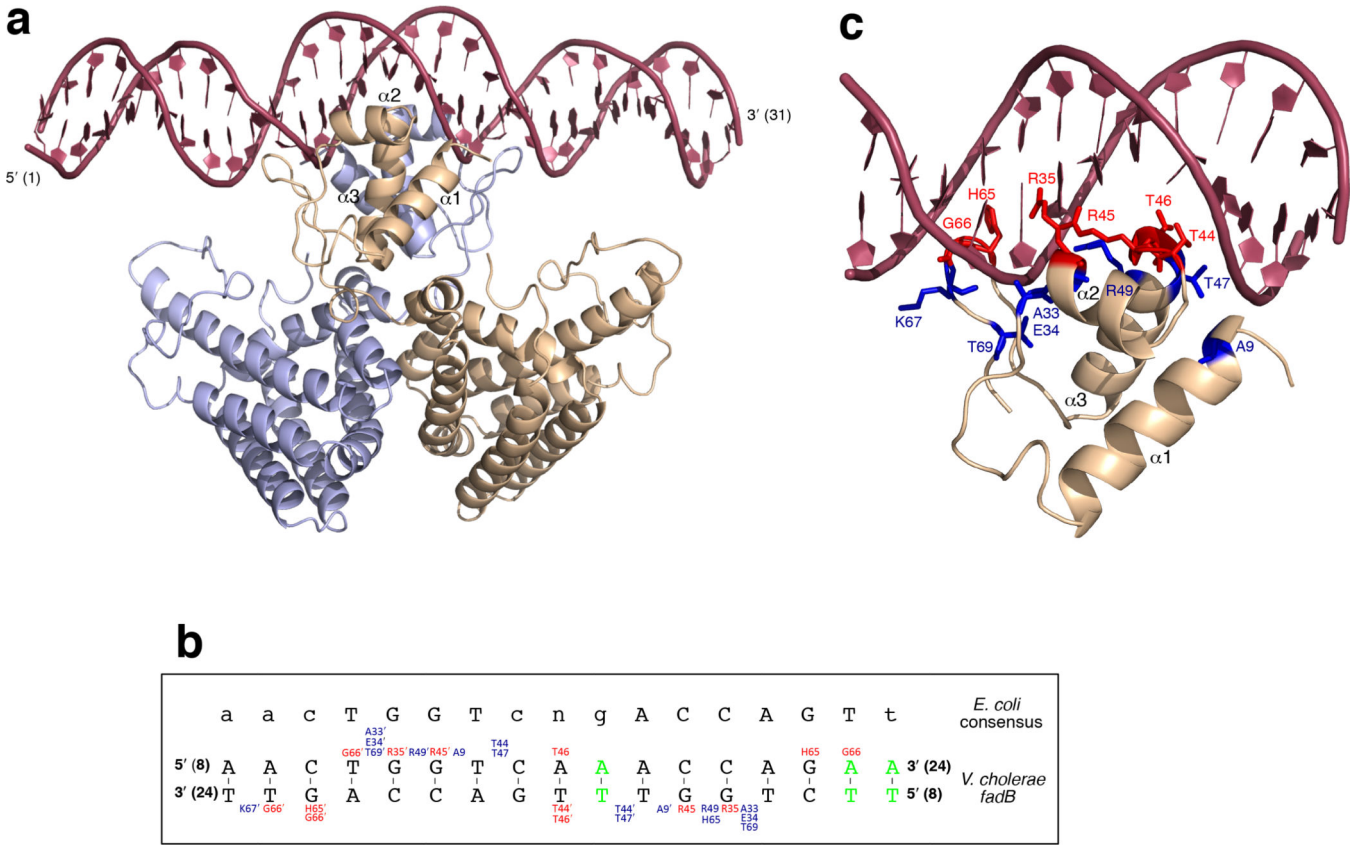

Figure 4. Structure of the *Vc*FadR-DNA complex

(a) The *Vc*FadR dimer bound to DNA. One monomer is slate blue and the other is wheat. (b) Schematic overview of the *Vc*FadR-DNA contacts. Residues that form specific contacts with the DNA are red and those that form nonspecific interactions with the DNA sugar-phosphate are dark blue. The base pairs in the *V. cholerae fadB* recognition sequence that are different from the *E. coli* consensus sequence[43] are green. Within the consensus sequence, upper and lowercase letters represent nucleotides found more and less frequently, respectively. Residues from chain B are distinguished by a prime following the amino acid number. (c) Stereoview showing a close up of the *Vc*FadR-DNA interface within one monomer. Colors are the same as in (b).

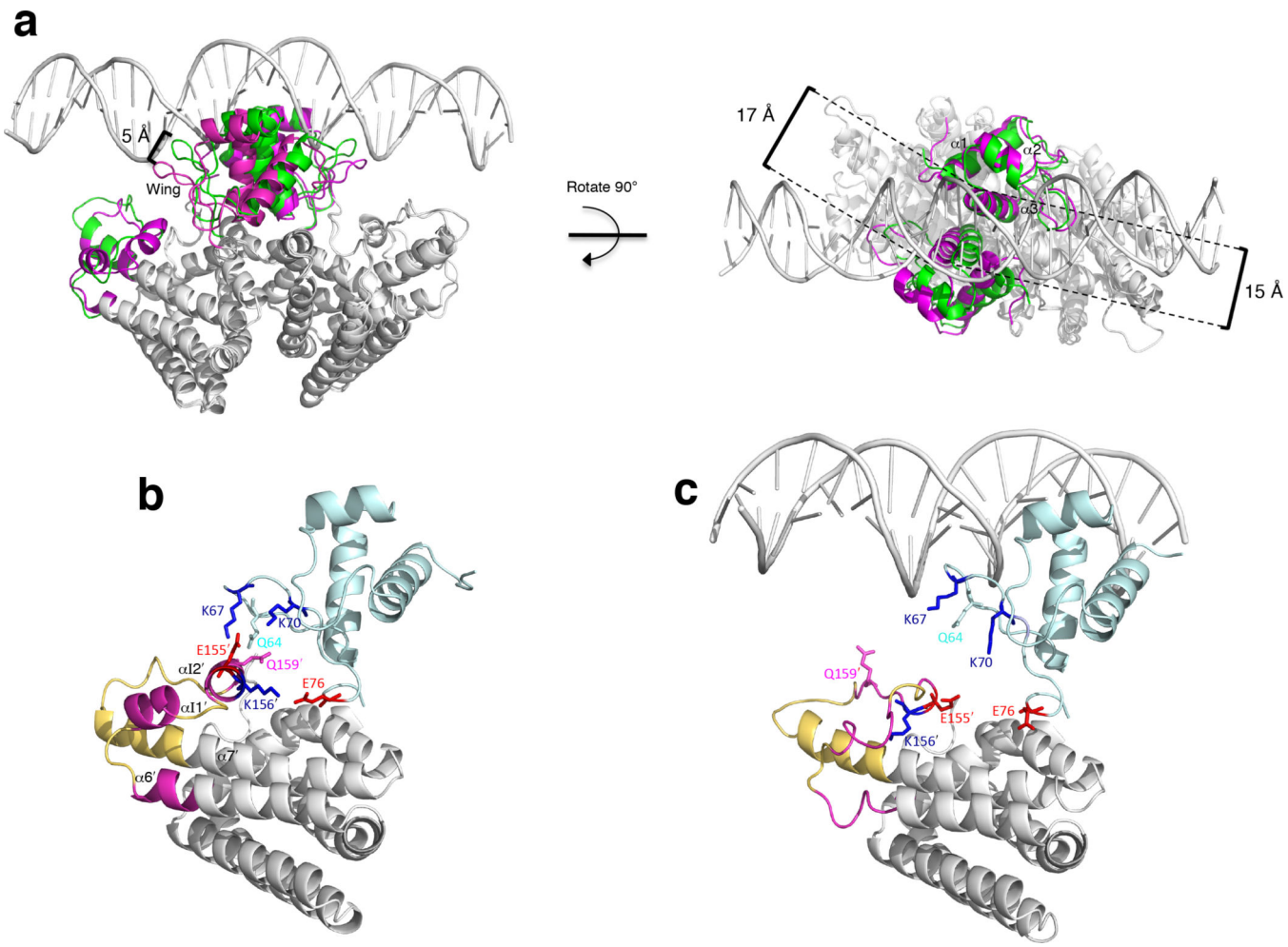

Figure 5. Conformational changes in *Vc*FadR upon DNA binding

(a) Superposition of the *Vc*FadR-DNA complex and apo-*Vc*FadR shown in two orientations (along and perpendicular to the pseudo 2-fold axis). The two primary regions that are altered upon DNA binding are shown in color (green, *Vc*FadR-DNA complex; magenta, apo-*Vc*FadR) and the rest of the protein is white. The tip of the wing (H65) in each DNA wHTH binding domain is shifted by up to 5 Å between the two structures and the distance between the two DNA recognition helices (R45 at the beginning of helix α3) is wider in apo-*Vc*FadR structure (17 Å) compared to that in the *Vc*FadR-DNA complex (15 Å). (b) Detailed view of the interaction between the insertion region and the wing of wHTH in the absence of the DNA. The N-terminal DNA binding domain is pale cyan. The region that undergoes a helix to loop transition upon DNA binding (helices αI1, αI2 and the C-terminal end of α6 in apo-*Vc*FadR) is magenta and the rest of the 40-residue insertion region is yellow. Residues that are positively charged are blue and those that are negatively charged are red. Helices and residues from chain B are distinguished by a prime. (c) Same view as in (b) but in the presence of DNA. The colors are the same as in (b).

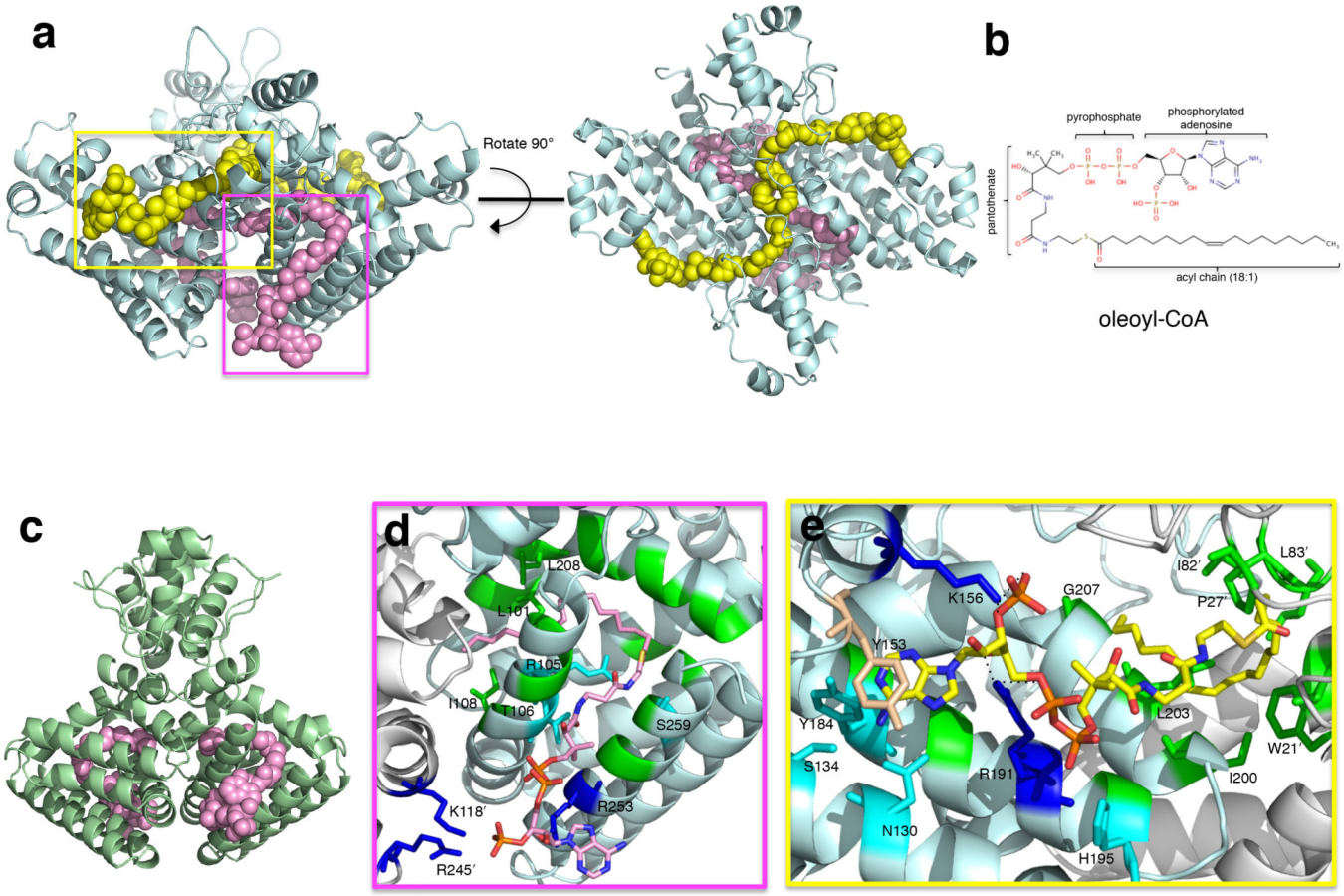

Figure 6. Structures of *Vc*FadR and *Ec*FadR with ligand

(a) The *Vc*FadR-oleoyl-CoA complex in two orientations. The ligand in the site corresponding to *Ec*FadR (see c) is shown in pink spheres whereas the ligand in the site that involves the insertion is in yellow spheres. (b) The chemical structure of oleoyl-CoA. (c) Structure of *Ec*FadR bound to myristoyl-CoA (PDB 1H9G)[16]. (d–e) Regions boxed in (a) highlighting critical residues interacting with the ligand in the pocket of *Vc*FadR corresponding to that of *E. coli* (d, site #1, monomer A) and in the pocket derived from the insertion (e, site #2, monomer A). Positively charged residues that interact with ligand phosphates are in blue. Residues forming hydrogen bonds are cyan, and those forming hydrophobic interactions are in green. Y153, which forms π-stacking with adenosine of the ligand, is wheat. Residues from chain B are distinguished by a prime following the amino acid number. The ligand is shown as sticks in (d) and (e). The carbon atoms are colored pink in (d) and yellow in (e). Other atoms of the ligand are colored as follows: nitrogen, blue; oxygen, red; sulfur, dark yellow; phosphorous, orange.

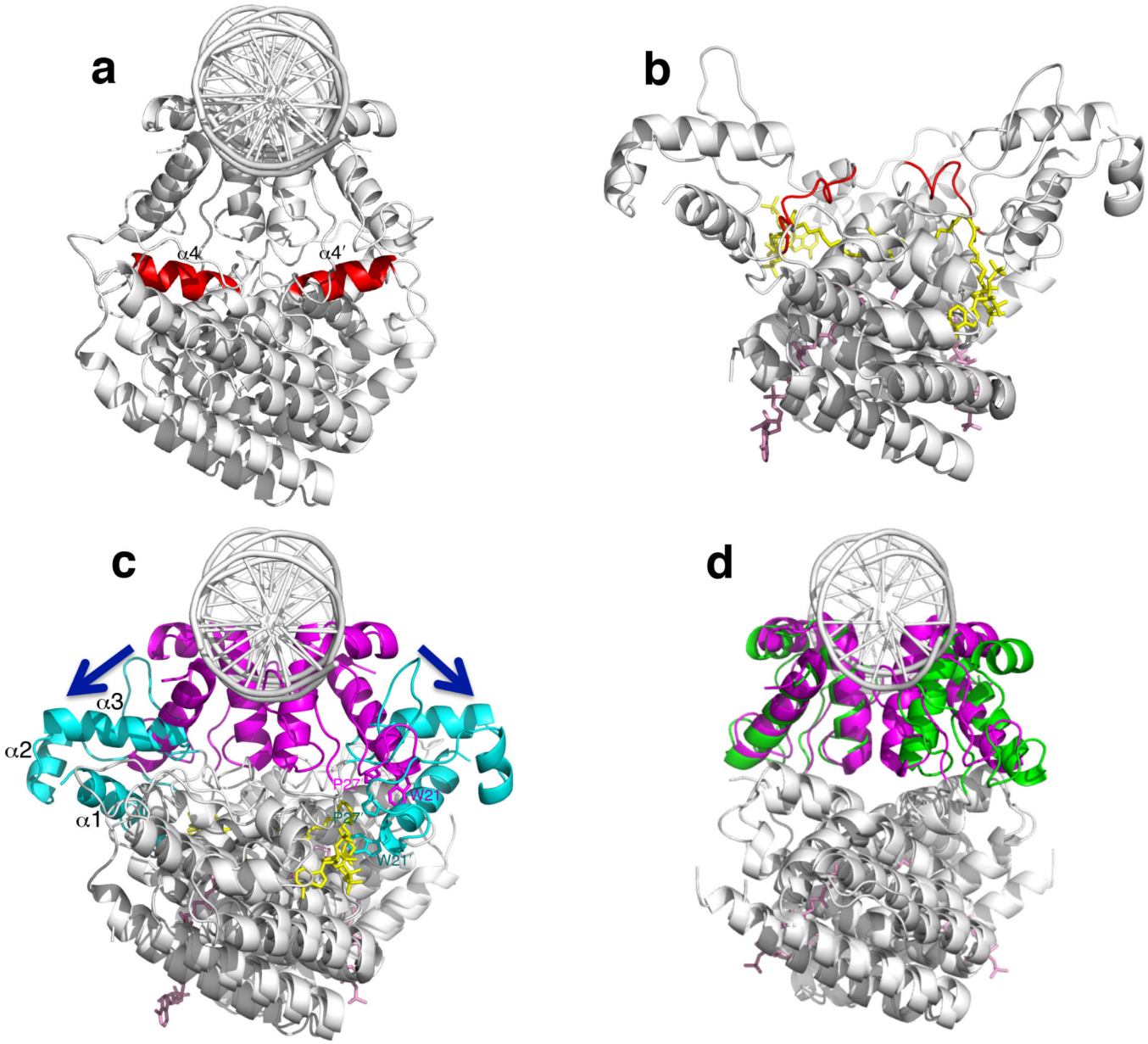

Figure 7. Comparison of effector mediated conformational changes between *V. cholerae* and *E. coli*

(a) The *Vc*FadR-DNA complex. The linker helix α4 is red and changes to a loop in the *Vc*FadR-ligand complex (b). α4 from chain B is distinguished by a prime. (c) Superposition of the structures of *Vc*FadR-DNA complex and *Vc*FadR-ligand complex. The DNA binding domain is in magenta (*Vc*FadR-DNA complex) or cyan (*Vc*FadR-ligand complex) and the rest of the protein is white. The arrows show that, upon ligand binding, the DNA binding domain is widened to almost 180°. Residues from chain B are distinguished by a prime following the amino acid number. (d) Superposition of the structures of *Ec*FadR-DNA complex (PDB 1H9T)[16] and *Ec*FadR-ligand complex (PDB 1H9G)[16]. The DNA binding

domain is magenta (*Ec*FadR-DNA complex) or green (*Ec*FadR-ligand complex) and the rest of the protein is white.

Table 1

Data collection and refinement statistics

	*Vc*FadR	*Vc*FadR-DNA	*Vc*FadR-oleoyl-CoA
Data collection			
Space group	$P4_1$	P1	$P2_12_12_1$
Cell dimensions			
a, *b*, *c* (Å)	87.48 87.48 81.43	84.6 94.7 101.7	116.92 88.69 62.86
α, β, γ, (°)	90 90 90	89.8 114.6 116.5	90 90 90
Resolution (Å)	19.56–2.20 (2.28–2.20)[a]	19.89–3.21 (3.32–3.21)	19.73–2.80 (2.90–2.80)
V_M(Å^3//Da)/solvent content (%)	2.4/49.7	3.9/71.0	2.4/48.4
No. of dimers in asymmetric unit	1	2	1
R_{sym}	7.9 (49.3)	8.9 (36.6)	13.1(48.3)
I / σI	33.8 (6.6)	13.0 (3.0)	11.5 (3.2)
Completeness (%)	99.8 (100.0)	97.8 (97.1)	99.7(99.6)
Redundancy	15.3 (15.2)	3.5 (3.5)	3.6 (3.7)
Refinement			
Resolution (Å)	19.56–2.2	19.89–3.21	19.73–2.8
No. reflections	31200	40186	16577
R_{work} / R_{free}	0.174/0.205	0.218/0.252	0.259/0.298
No. atoms			
Protein	4488	4402	4240
Ligand/DNA	-	1271	268
Water	387	-	-
B-factors (Å^2)			
Wilson B-factor	25.9	73.3	35.7
Protein	27.0	83.7	74.1
Ligand/DNA	-	98.5	59.5
Water	30.30	-	-
R.m.s. deviations			
Bond lengths (Å)	0.004	0.007	0.010
Bond angles (°)	0.9	1.4	2.2

Each dataset was collected from a single crystal.

[a]Values in parentheses are for highest-resolution shell.